Investigation of the liquid accumulation characteristics in planar prefilming airblast atomization

G. Chaussonnet*, T. Laroche, C. Lieber, S. Holz, R. Koch, H.-J. Bauer

Karlsruher Institut für Technologie (KIT), Karlsruhe, Germany
Institut für Thermische Strömungsmaschinen
*geoffroy.chaussonnet@kit.edu

Abstract

The phenomenon of prefilming airblast atomization is investigated by means of shadowgraphy. The focus is on the liquid accumulation, which is attached to the trailing edge in the wake region of the prefilmer. The prefilmer is planar to facilitate the measurements, and the trailing edge thickness is 230 µm. The investigated liquid is a kerosene surrogate (Shellsol D70). The operating parameters are varied with a bulk gas velocity ranging from 20 to 100 m/s and a surface volumetric liquid flow rate ranging from 20 to $120\,\mathrm{mm}^2/\mathrm{s}$. In order to statistically investigate the liquid accumulation, it is virtually split into several atomizing cells. Each cell consists of a single ligament and a surrounding liquid part. Different characteristic lengths of the atomization cells are extracted by a in-house post-process tool. The distribution of these length scales are well described by a gamma function, whose scale parameter m is proportional to a Weber number based on the trailing edge thickness ($\mathrm{We}_{\mathrm{te}}$). However, it is observed that the parameter m also varies with the liquid flow rate, independently of $\mathrm{We}_{\mathrm{te}}$. A two-step mechanism is proposed for the dynamics of the liquid accumulation, leading to the expression of a new length scale, which combines $\mathrm{We}_{\mathrm{te}}$ and the liquid flow rate. It is observed that the prediction of this new length scale is in good agreement with the experiment. Hence, this new characteristic length is a good candidate for predicting the length scale of the accumulation in more general configurations.

Keywords: prefilming airblast atomization, shadowgraphy measurement, liquid accumulation

---

Introduction

Prefilming airblast atomizers are commonly used to inject liquid fuel into the combustion chamber of gas turbines. Applied to aircraft engines, this type of injector exhibits stable performances on a wide range of operating conditions [1]. Despite its advantages, prefilming airblast atomization is still not fully understood. At the beginning of the XXI century, prefilming airbast atomization was not conceptually distinguished from general other types of atomization such as the breakup of a liquid sheet or of a cylindrical jet, the common aspect being the fragmentation of the liquid by the high-speed air stream. Several models were derived to predict the spray characteristics [2, 3] of prefilming airblast atomization, based on the characteristics of the film flow on the prefilmer.
Since 2010, the work of Gepperth *et al.* [4, 5, 6] and Müller [7] showed that the characteristics of the spray is decoupled from the film flow over a wide range of operating parameters. Moreover, they provided evidences suggesting that the key of prefilming airblast atomization lies in the volume of liquid that accumulates at the tip of trailing edge, in the wake region of the prefilmer. This liquid accumulation was originally mentioned by Sattlemayer *et al.* [8] but the measurement techniques in those days forbade any precise quantification of its influence on the spray characteristics. Gepperth *et al.* [5] showed that the SMD of the spray was proportional to thickness of the trailing edge. Based on this observation, Chaussonnet *et al.* [10] proposed a model to predict the size distribution of the droplets. The application of the Smoothed Particle Hydrodynamics (SPH) method to a 2D case of the configuration also showed the influence of the trailing edge thickness on the breakup events [9]. Recently Warncke *et al.* [11] provided a numerical analysis on the liquid accumulation and Okabe *et al.* [12] also investigated experimentally the influence of the trailing edge thickness on the dynamics of the liquid accumulation.

The present study focuses on the geometrical characteristics of the liquid accumulation and propose a scenario to predict the dimension of the liquid accumulation based on the operating parameters. The experiment is presented in the first section, followed by a description of the post-processing tool. Results of the experiment are shown in a third part, and finally, a mechanism on the evolution of the accumulation is proposed and compared to the experiment.

Experimental apparatus

The experience was conducted at the spray test-rig at the Institut für Termische Strömungsmaschinen (ITS), as in [5]. The air is supplied by a compressor whose maximal mass flow rate is $80\,\mathrm{g}/\mathrm{s}$, monitored by a hot-wire.

A flow straigthener is mounted upstream the prefilmer to ensure a fully turbulent and non-swirling flow, and a nozzle is positioned at the prefilmer inlet to reduce any hazards of boundary layer detachment. The temperature is recorded upstream the flow straightener.
The liquid, a kerosene surrogate (Shellsol D70), is stored in a vessel pressurized to ≈2 bar, and the liquid mass flow rate is controlled by a Coriolis flow-meter. The flow exiting the atomizer is sucked by a vacuum pump to reproduce the flow pattern of a real combustion chamber, and to ensure a measurement volume free of recirculating droplets. An honeycomb structure is positioned 60 cm downstream the prefilmer to prevent droplets from being trapped in residual recirculation zones. The liquid is then separated from the gas phase in a cyclone.

Geometry

The atomizer is a planar abstraction of an annular airblast injector (Fig. 1), similar to the one investigated in [5]. It consists of a prefilmer made of 3D extrusion of a wing-shape profile in Perspex material. The liquid is injected on the prefilmer via 50 equidistant holes of 0.5 mm each, distributed in the transverse direction (Y in Fig. 1). The liquid uniformly wets the prefilmer surface and forms a thin liquid film. The film is sheared by the high speed air stream to the trailing edge where it accumulates in wake region induced of the prefilmer. Then, the liquid accumulation is torn by the air and exhibits structures similar to bag breakup and to ligament breakup.

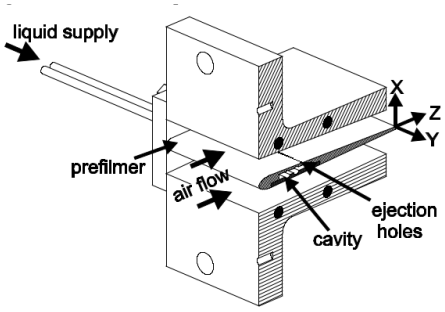

Figure 1 Schematic of the test section, from [5]

All the geometric parameters of the prefilmer are indicated on Fig. 2, and their values are summariezd in Table 1. The large aspect ratio of the channel ensures a negligible effect of the corner vortices on the film flow and the liquid accumulation, on the center line of the geometry.

Operating conditions

All measurements were conducted at atmospheric pressure and a temperature between 19 and 29°C. The mean gas velocity was determined by the continuity based on the channel surface S=WH and the density given by the gas temperature upstream the atomizer. It was varied from 20 to $100\,\mathrm{m/s}$. The liquid mass flow rate was varied from 0.77 to $4.62\,\mathrm{g/s}$, corresponding to a film loading Λ_f from 20 to $120\,\mathrm{mm^2/s}$. All values are summarized in Table 2.

Measurement techniques

The accumulation was investigated by means of shadowgraphy. A double pulse Nd:YAG laser with 140 mJ per pulse was used as a light source. Each light pulse was diffused and spatially expanded to provide homogeneous background illumination. The receiving optic consists of an objective mounted on a high resolution CCD camera. The characteristics of the objective are a focal length f of $200\,\mathrm{mm}$ and an opening of $f/8$, and the resolution of the

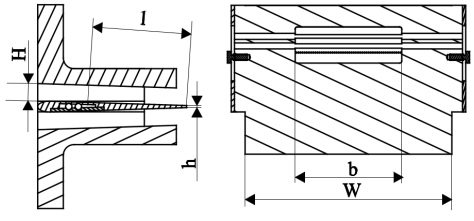

(a) *XZ*-plane (b) *YZ*-plane

Figure 2 Value of the geometrical parameter, from [5].

prefilming length	l	[mm]	47.6
trailing edge thickness	h	[µm]	230
prefilming width	b	[mm]	50
air channel height	H	[mm]	8.11
air channel width	W	[mm]	96
prefilmer chord length	L_C	[mm]	71.4

Table 1 Value of the geometrical parameter

Density ρ_g $[\mathrm{kg\,m^{-3}}]$	Dyn. Visc. μ_g $[\mathrm{Pa\,s}]$	Temperature T $[\mathrm{K}]$	Mean velocity U_g $[\mathrm{m\,s^{-1}}]$	Density ρ_l $[\mathrm{kg\,m^{-3}}]$	Dyn. Visc. μ_l $[\mathrm{Pa\,s}]$	Surface tension σ $[\mathrm{N\,m^{-1}}]$	Film loading Λ_f $[\mathrm{mm^2\,s^{-1}}]$
1.2	1.8×10^{-6}	293-303	20-100	770	1.56×10^{-3}	0.0275	20-120

Table 2 Experimental parameters and test conditions.

CCD camera is 1600 by 1200 pixels. In the measurement conditions, the pixel size was $13.0\,\mu\mathrm{m}$ and the Depth-of-Field was $8\,\mathrm{mm}$. The field of view was $20.72\,\mathrm{mm}$ in the axial direction and $15.54\,\mathrm{mm}$ in the transverse direction. For each operating point, 200 double frame images were taken at a sampling frequency of 30 Hz. The time delay between the two frames of a single picture was $50\,\mu\mathrm{s}$, ensuring a decoupling between the two frames. Hence, in total, 400 frames were taken per operating point.

Post-processing procedure

The snapshots were automatically processed by a in-house code [13], which proceeds in two steps as illustrated in Fig. 3. First, the liquid accumulation is extracted by a contour recognition algorithm, depending on a threshold based on the pixel median value, for each snapshot. Then, the crests (red arrows) and troughs (yellow arrows) of the contour are detected from the inflexion point of the contour line (Fig. 3 left).
Because the contour line of the liquid accumulation is very perturbed, crests and troughs can be detected without any significance for a real ligament. Hence, they are filtered out based on geometric criteria, which will be explained in detail later.

The remaining crests and troughs define the subdomains of the liquid accumulation (Fig. 3 right). These are referred to as *atomizing cell* in the following, and correspond to colored areas in Fig. 3 right).

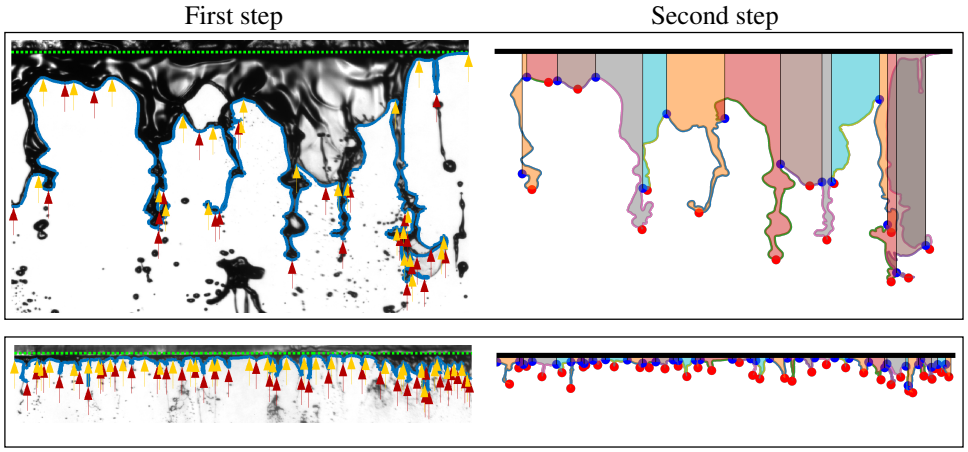

Figure 3 Illustration of the post-process workflow, for $U_g = 20\,\mathrm{m/s}$ and $\Lambda_f = 120\,\mathrm{mm^2/s}$ (top) and $U_g = 100\,\mathrm{m/s}$ and $\Lambda_f = 20\,\mathrm{mm^2/s}$ (bottom).

From each atomizing cell several quantities are extracted, as depicted on Fig. 4. First, the ligament length l_0 is taken as the distance between the trailing edge and the maximum axial extent of the ligament. Second, the cell width w_0 is defined as the transverse extent of the atomizing cell. Finally, the streamwise surface d_0^2 is equal to the area of the atomizing cell, projected on the (YZ) plan.

All of the three quantities are collected for each operating point, leading to a number of samples between 1800 and 22000, for low and high air velocity, respectively.

The filtering of the crests and troughs is a critical point that deserve more explanations. Depending on the filtering criteria, the atomizing cells might exhibits different geometrical characteristics. Therefore filtering criteria were based on the following principles:

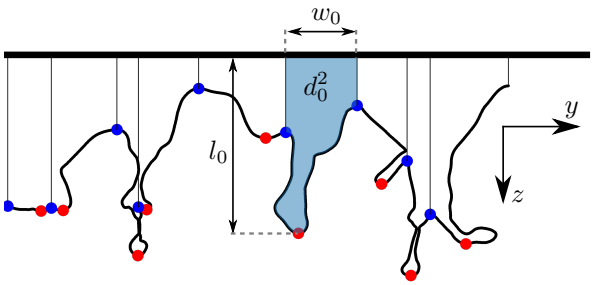

Figure 4 Illustration of geometrical quantities extracted for each atomizing cell.

1. the liquid is sheared by the gas and elongated axially, so that the crest is further from the trailing edge than the troughs:$z_{cr} > z_{tr,i}$.
2. since the crest is elongated axially, its transverse position should remain the boundaries of the cell, *i.e.* in between the two troughs: $y_{tr,1} < y_{cr} < y_{tr,2}$.
3. the area is computed from the circulation on a closed contour and therefore is a signed quantity, depending on the direction in which the loop is followed. The filtering algorithm computes the area to obtain a positive area. If a negative area is found, it means that the shape of the ligament is too distorted or incomplete. Hence: $d_0^2 > 0$
4. the area of an atomizing cell must be larger than the area delimited by the troughs: $d_0^2 > w_0\,(z_{tr,1} + z_{tr,2})/2$

It is observed in Fig. 3 (top right) that the post-processing procedure can sometimes lead to unrealistic large area d_0^2. However, these artifacts occur seldom and they are smoothed out due to the larger number of samples.

Results and Discussion

Qualitative analysis

Figure 5 summarizes the regimes observed in the different operating conditions. The snapshots are disposed so that one column represents a constant velocity and one row represents a constant film loading. As mentioned by Gepperth *et al.* [5], the gas velocity is one of the more important parameters, as it sizes the length of a ligament, almost independently of the film loading. However, when considering the liquid accumulation, *i.e.* the space filled with liquid between the trailing edge and the foot of the ligament, the influence of the film loading is visible, together with the gas velocity. Indeed, when the film loading increases, the axial extent of the accumulation increases, and the amplitude of the growth depends on the gas velocity. Therefore, there is a crossed influence of the gas velocity and the film loading with regards to the liquid accumulation.
It is to be highlighted that both ligament and bag breakups are observed at any film loadings and gas velocities. However, ligament breakup is more frequent compared to bag breakup when the film loading and the gas velocity are both low.

Quantitative analysis

The probability density functions of the ligament length l_0, the atomizing cell width w_0 and surface-based length d_0 are shown in Fig. 6 for U_g = 40 and 100 m/s and all film loadings. Globally, the three extracted quantities show a dependance on the film loading with a shift of their peak. This shift is more pronounced at lower velocity. When the film loading increases, the peak of l_0 moves towards larger values and its dispersion increases. The complete opposite behavior is observed for w_0. The length scale d_0 based on the area shows the advantage to depend little on the film loading. Moreover, the relative evolution of its PDF with the film loading is also almost independent of the gas velocity.

The PDF of each value was fitted by four usual functions, log-normal, root-normal, Rosin-Rammler and gamma. Even though the shape of the PDF are very smooth and were relatively well fit by all the test distributions, the gamma distribution G provided the best fit. It is illustrated in Fig. 7 (left). The Gamma distribution is expressed as:

$$G(x) = \frac{q^q}{\Gamma(q)}\, x^{q-1} e^{-q\,x} \quad \text{with} \quad x = d/m \tag{1}$$

where m and q are called the scale and shape parameter, respectively. The term Γ is the Gamma function. Since d_0 is less dependent to the operating conditions than l_0 and w_0, it is investigated in the following. The dependence of

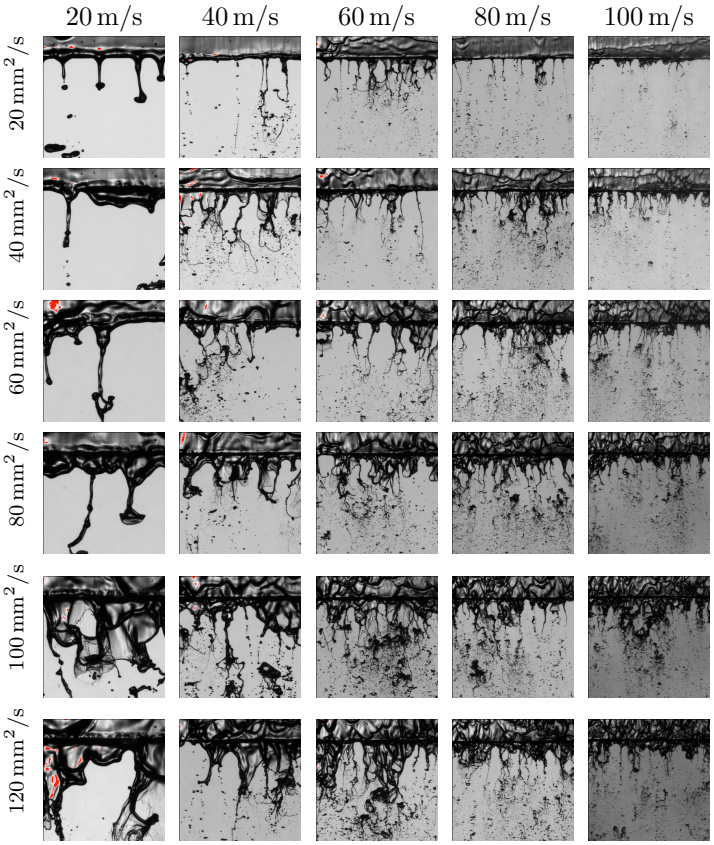

Figure 5 Snapshots of liquid accumulation breakup. The column and row titles correspond to U_g and Λ_f, respectively.

m and q on the film loading and the gas velocity are depicted in Fig. 7 (right). The scale parameter exhibits a clear monotonic dependence on the film loading and the gas velocity, as observed in the experiment (Fig. 5). Concerning the shape parameter, which depicts the dispersion of d_0, it decreases with an increasing Λ_f and a decreasing U_g, even though the evolution is not always monotonic for a low U_g and a large Λ_f.

Scenario for the liquid accumulation

An attempt to give a physical explanation for the representativeness of d_0 is provided in the following, based on a ratio of stabilizing and destabilizing forces applied to an atomizing cell, and depicted in Fig. 8. In the liquid accumulation, the stress due to the surface tension is of the order σ/h, and it is applied to a surface proportional to h^2 (Fig. 8 left). It is assumed that when the ligament is elongated axially, this approximation is still valid, even though the area of the curved surface decreases. Concerning the aerodynamic stress (Fig. 8 right), it is estimated by $\rho_g\, U_g^2/2$ and it applies on the surface in contact with the air stream, which is equal to d_0^2 by definition. Hence, the stabilizing force f_{st} due to surface tension and the destabilizing force f_{aero} due to the aerodynamic stress can be expressed as:

$$f_{st} \propto \sigma\, h \quad \text{and} \quad f_{aero} \propto \rho_g\, d_0^2\, U_g^2 \tag{2}$$

The ratio of theses force lead to a Weber number based on two length scales h and d_0: $\mathrm{We}_2 = \rho_g\, U_g^2\, d_0^2/(\sigma\, h)$ By defining the *most frequent* Weber number We_2^0 based on the peak value in the PDF of d_0 (labeled here <d_0>), $\mathrm{We}_2^0 = \rho_g\, U_g^2\, \langle d_0 \rangle^2/(\sigma\, h)$, we obtain the relation:

$$\langle d_0 \rangle \;\propto\; \sqrt{\frac{\sigma\, h}{\rho_g\, U_g^2}}\, \sqrt{\mathrm{We}^0} \tag{3}$$

In the following, the signs $\langle\rangle$ are dropped for the sake of clarity. By assuming that We^0 is a constant independent of the operating conditions, we can express the ratio d_0/h as:

$$d_0/h \;\propto\; 1/\sqrt{\mathrm{We}_{te}} \quad \text{where} \quad \mathrm{We}_{te} = \rho_g\, U_g^2\, h/\sigma \tag{4}$$

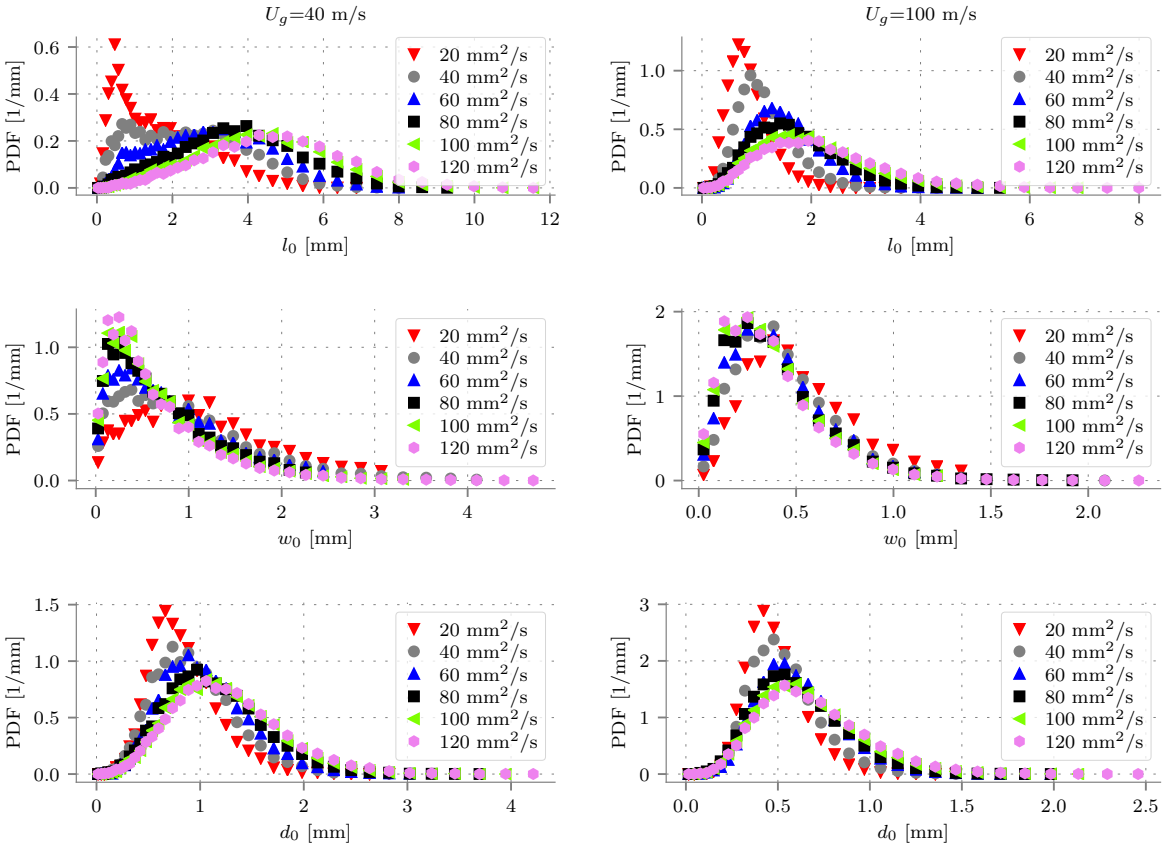

Figure 6 Probability density functions of l_0, w_0 and d_0 for U_g = 40 m/s (left) and 100 m/s (right).

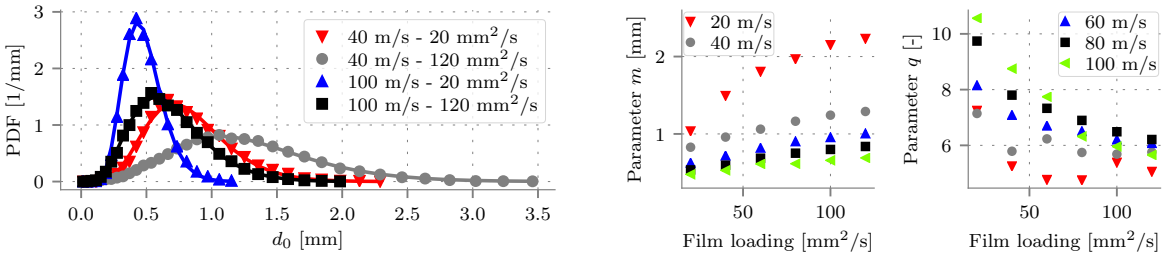

Figure 7 Left: Probability density functions of d_0 superimposed with the gamma function. Right: parameters m and q versus the film loading for different mean gas velocity.

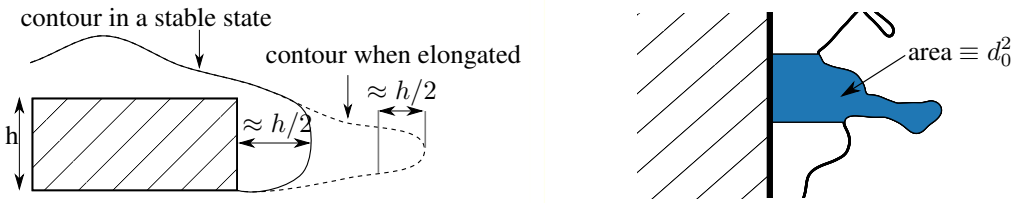

Figure 8 Sketch of surface tension (left, side view) and the aerodynamic stress (right, top view) applied to the liquid accumulation.

The evolution of d_0/h versus $1/\sqrt{\mathrm{We}_{te}}$ is depicted on Fig. 9 and exhibits a linear correlation, whose slope depends on the film loading. Indeed, Eq. 4 does not depends on Λ_f whereas the influence of the film loading is clearly visible on the parameter m in Fig. 8 (right). In order to take the film loading into account, a two-step mechanism

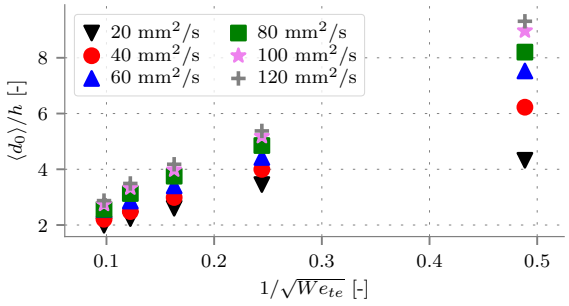

Figure 9 Comparison of d_0/h form the fitting by the Gamma distribution versus $1/\sqrt{\mathrm{We}_{te}}$.

is considered and illustrated in Fig. 10. It consists in the filling in (step 1) and the breakup (step 2) of the liquid accumulation. The initial state is a bare trailing edge with no liquid, *i.e.* no accumulation (i). The liquid starts to accumulates in the wake zone of the prefilmer and thus remains in a stable form (ii). After the time necessary to fill in the accumulation to its maximum stable form (iii), the accumulation starts to be stretched axially (iv). This results in the formation of a ligament (v) which is finally torn apart from the liquid accumulation (vi). During the second step (iv to vi), the liquid film continuously feeds the accumulation, so that the volume of the ligament to be fragmented is larger than the volume of the stable atomizing cell.

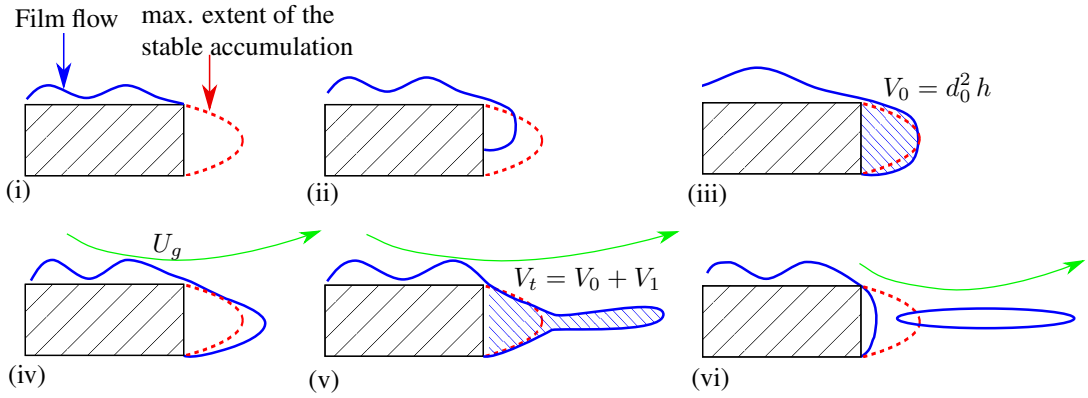

Figure 10 Proposed scenario for the breakup of the liquid accumulation.

According to Marmottant & Villermaux [14], the breakup time of a ligament is weakly dependent on the rate of elongation and depends mostly on the initial ligament volume. It is proportional to the capillary time $t_\sigma = \sqrt{\rho_l\, V_0/\sigma}$ where V_0 is the initial volume of the ligament to be fragmented, corresponding to the volume of the stable atomizing cell. It is estimated by $d_0^2\, h$, leading to a breakup time t_{bu}:

$$t_{bu} \;\propto\; \frac{h}{U_g}\sqrt{\frac{\rho_l}{\rho_g}} \tag{5}$$

The striking point of Eq. 5 is that t_{bu} is independent of the surface tension. This results must be consolidated with different types of liquid.
During the elongation of the ligament, the film injects a volume of liquid equal to $V_1 = C_1\, d_0\, \Lambda_f\, t_{bu}$ where C_1 is a constant to be determined. This means that the total volume V_t of the atomizing cell which consists of the accumulation and the ligament, and it is equal to $V_t = V_0 + V_1$. In order to estimate the length scale of the atomizing cell as previously, we define the total volume as a streamwise surface multiplied by the prefilmer thickness $V_t = d_1^2\, h$ which leads to the definition of the total length scale d_1.
To summarize, d_1 is determined from the following equations:

$$d_1 = \sqrt{V_t/h} \quad \text{with} \quad V_t = d_0^2\, h + d_0\, \Lambda_f\, t_{bu}\,, \quad d_0 = \sqrt{\frac{\sigma\, h}{\rho_g\, U_g^2}} \quad \text{and} \quad t_{bu} = C_1 \frac{h}{U_g}\sqrt{\frac{\rho_l}{\rho_g}} \tag{6}$$

Figure 11 shows the estimation of d_1/h versus m/h, with the constant C_1 equal to 3. The agreement is very good, for all mean gas velocity and all film loading, except for large values of d_1/h, which correspond to U_g=20 m/s where the breakup mechanism is close to a transition regime.

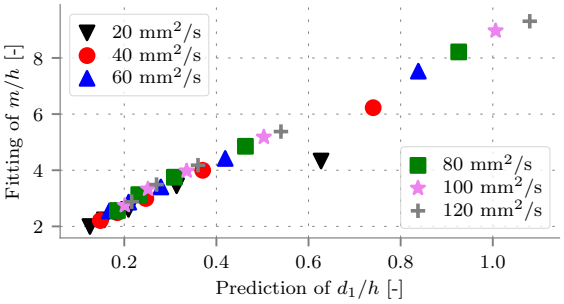

Figure 11 Prediction of d_1/h versus m/h.

Conclusion

In this paper, the liquid accumulating at the trailing edge of a planar prefilming airblast atomizer was investigated by means of shadowgraphy. The mean air velocity and the film loading were independently varied. An in-house post-processing tool was applied to separate the liquid accumulation from the fragmented structures, and the accumulation was split into elementary liquid units referred to as *atomizing cells*. Several geometrical quantities were extracted from the atomizing cell and their distribution was well described by the gamma function. Additionally, the length scale d_0 based on the atomizing cell streamwise surface showed the most stable behavior versus the variation of operating parameters, compared to other geometric quantities. An attempt to give a physical explanation to d_0 was realized and showed a good agreement with regard to the air velocity. Finally, a two-step scenario for the filling and stretching of the liquid accumulation was proposed, which led to the definition of a new length scale d_1 that take the film loading into account. This new length scale showed also a good scaling versus the air velocity and the film loading.
In the future, the proposed mechanism will be investigated versus the trailing edge thickness and the surface tension, the final goal being to use d_1 as a generating value to predict the SMD of the spray.

References

[1] Lefebvre, A. H., *Atomization and Sprays*, 10(3-5) (2000).
[2] Inamura, T.; Shirota, M.; Tsushima, M.; Kato, M.; Hamajima, S. and Sato, A., *ICLASS, 12th Triennial International Annual Conference on Liquid Atomization and Spray Systems* (2012).
[3] Eckel, G.; Rachner, M.; Le Clercq, P. and Aigner, M., *8th International Conference on Multiphase Flow* (2013).
[4] Gepperth, S.; Guildenbecher, D.; Koch, R. and Bauer, H.-J., *International Conference for Liquid Atomization and Spray Systems*, ILASS-Europe, Brno, Czech Republic (2010).
[5] Gepperth, S.; Müller, A.; Koch, R. and Bauer, H.-J., *ICLASS, 12th Triennial International Annual Conference on Liquid Atomization and Spray Systems*, Heidelberg, Germany (2012).
[6] Gepperth, S.; Koch, R. and Bauer, H.-J., *ASME Turbo Expo 2013: Turbine Technical Conference and Exposition*, American Society of Mechanical Engineers (2013).
[7] Müller, A., *Experimentelle Untersuchung des Zerstäubungsverhaltens luftgestützter Brennstoffdüsen bei oszillierenden Strömungen*, Ph.D. thesis, Karlsruhe Institute of Technology (2015).
[8] Sattelmayer, T. and Wittig, S., *Journal of engineering for gas turbines and power*, 108(3):465–472 (1986).
[9] Braun, S.; Wieth, L.; Koch, R. and Bauer, H.-J., *Proceedings of the International Conference on Liquid Atomization and Spray Systems (ICLASS)* (2015).
[10] Chaussonnet, G.; Vermorel, O.; Riber, E. and Cuenot, B., *International Journal of Multiphase Flow*, 80:29–42 (2016).
[11] Warncke, K.; Gepperth, S.; Sauer, B.; Sadiki, A.; Janicka, J.; Koch, R. and Bauer, H.-J., *International Journal of Multiphase Flow*, 91:208–224 (2017).
[12] Okabe, T.; Katagata, N.; Sakaki, T.; Inamura, T. and Fumoto, K., *Proceedings of the International Conference on Liquid Atomization and Spray System (ILASS)* (2017).
[13] Müller, A.; Dullenkopf, K. and Bauer, H.-J., *14th Int. Symp. on Applications of Laser Techniques to Fluid Mechanics* (2008).
[14] Marmottant, P. and Villermaux, E., *Journal of Fluid Mechanics*, 498:73–111 (2004).